Effect of the microstructure on the tribological properties of HIPed and PTA-welded Fe-based hardfacing alloy

M.R. Ardigo-Besnard, A. Tellier, A. Besnard, J.-P. Chateau-Cornu

Version of Record: https://www.sciencedirect.com/science/article/pii/S0257897221008653
Manuscript_aa8ae1b229912b24b10ff2d4b2e54e5d

Effect of the microstructure on the tribological properties of HIPed and PTA-welded Fe-based hardfacing alloy.

M. R. Ardigo-Besnard[1,a], A. Tellier[a], A. Besnard[b], J.-P. Chateau-Cornu[a]

[a]*Laboratoire Interdisciplinaire Carnot de Bourgogne (ICB), UMR 6303 CNRS, Univ. Bourgogne Franche-Comté, BP 47870, 21078 DIJON Cedex, France*

[b]*Arts et Metiers Institute of Technology, LaBoMaP, HESAM Université, 71250 Cluny, France*

Abstract

This work focuses on the comparison of the tribological properties of Norem02, a Fe-based hardfacing elaborated by hot isostatic pressing (HIP), a pressure-assisted sintering technique and by plasma transferred arc welding (PTAW), a more conventional coating process. The influence of the microstructural modifications induced by the elaboration process is investigated. The aim of the present study is to assess the possibility of considering HIP as an effective alternative to more conventional hardfacing techniques. Wear tests were carried out using a pin-on-disk tribometer with ball-on-plate configuration under loads of 2, 5 and 10 N against a WC-Co ball counterpart. The worn tracks present typical marks of abrasive wear followed by oxidative but also adhesive ones. HIPed sample presents a dominance of oxidative and adhesive wear, while for sample elaborated by PTAW the dominant mechanism is abrasive wear. The results indicate that in the case of the HIPed alloy the wear resistance is generally increased and under a load of 10 N the wear rate of the HIPed Norem02 is reduced of about 5.5 times. The fine microstructure obtained by HIP, containing small globular carbides well dispersed in the matrix allows the alloy to better withstand the mechanical stresses occurring during the wear tests, reducing the surface damages.

[1] Corresponding author. Tel.: +33 (0)380396016; fax: +33 (0)380396132.
E-mail address: maria-rosa.ardigo-besnard@u-bourgogne.fr

Keywords: hardfacing, coating, microstructure, wear resistance, friction, powder metallurgy, PTAW.

1. Introduction

Fe-based hardfacing alloys with high carbon and chromium contents possess good wear resistance properties in severe environmental conditions, such as high pressure, high temperature and corrosive atmosphere [1, 2]. Among all the Fe-based alloys, Norem02 is typically used as hardfacing for sliding components in nuclear power plants, where temperatures can range from 90 to about 300 °C under a normal contact stress of few hundreds MPa [3-5]. Several authors report that Norem02 elaborated by different techniques, such as laser processing, plasma transferred arc welding (PTAW), gas tungsten arc welding (GTAW) and laser-aided direct metal rapid tooling (DMT) process, presents satisfactory wear resistance properties at room temperature [2-4, 6]. This behaviour is explained by a low stacking fault energy (SFE) of the matrix [7], that suppresses the cross-slip of dislocations and then increases the work hardening rate of the alloy [8, 9]. Generally, the increase of the material hardness by work hardening improves the galling resistance, as observed in the case of the Norem02 [3, 10]. However, a significant degradation of the wear resistance properties of Norem02 is reported for temperatures higher than 150 °C, when adhesive wear becomes the dominant wear mechanism [3, 4]. Actually, the development of strain-induced martensite is considered of primary importance for the wear resistance of Norem02. The suppression of strain-induced phase transformation from austenite to martensite above 150 °C, known to be related to the increase of the stacking fault energy (SFE) of the matrix with temperature, is supposed to be one of the main reasons of the change in the dominant wear mechanism at high temperature and of the significant loss of the wear resistance of Norem02.

It is well known that the tribological behaviour of steels is influenced by their microstructure, particularly the size and the distribution of the hard phases, typically carbides [11-15]. Karlsson *et al*. [16, 17] showed that fine carbides, homogenously distributed into the matrix, typically enhance the wear performance of stainless and tool steels.

Ur Rahman *et al.* [18] reported that the wear resistance of high speed steel alloys is increased at 25 °C by a refinement of the microstructure. Malayoglu *et al*. [19] compared the performance of hot isostatically pressed (HIPed) and cast Stellite 6, a Co-based alloy. The HIPed alloy, composed of fine grains and small carbides dispersed into the matrix, presents a higher resistance to mechanical degradation (erosion and corrosion-erosion), compared to the cast material. The positive impact of a finer microstructure on the galling properties of some Fe-based alloys was also reported by Ohriner *et al*. [7]. Wong Kian *et al*. [20] compared the corrosion-erosion behaviour of HIPed and GTAW deposited Stellite coatings and showed that the HIP samples presented higher resistance than the welded ones.

Based on these literature results, it is possible to claim that HIP is an interesting elaboration process for the production of improved hardfacings for nuclear power plants, as the refinement of the microstructure of the Norem02 induced by HIP can represent a solution to improve the tribological properties of the alloy. The aim of this work is to give preliminary results, at laboratory scale, about the tribological properties of HIPed Norem02 and to show the opportunity of considering this powder metallurgy process as an effective alternative to more conventional hardfacing techniques, e.g. PTAW. The Norem02 powder is directly HIPed on the valve seat surface, which represents the surface to be coated and constitutes a part of the container. The wear resistance at room temperature of Norem02 elaborated by HIP and PTAW are investigated and friction mechanisms are compared.

2. Materials and methods

The Norem02 powder used in this study was supplied by Ducal. Its composition is 1.2 C – 24.8 Cr – 4.6 Mn – 3.5 Ni – 2.1 Mo – 3.0 Si – 0.027 O – bal. Fe (in wt.%). Morphological and chemical characterisations of the powder are reported in a previous work [21] and are not described here. The powder composition was reproduced in the nominal compositions of the HIP and PTAW hardfacings. The HIPed Norem02 samples were obtained by sintering at

1100 °C and 120 MPa for 3 hours, after a 2 hours heating and pressurizing ramp and natural cooling (process details are available in [22]). The Norem02 elaborated by PTAW was taken from an industrial pressurized water reactor (PWR) shutter for which precise process parameters are not of our knowledge. The thickness of the hardfacings was about two centimetres. The surfaces used for the tribological tests were free from any substrate influence (e.g. dilution). The samples were polished using SiC papers (down to 4000 grit), diamond paste (down to 1 µm), and colloidal silica (30 nm). Microstructures were characterised using a JEOL JSM-7600F scanning electron microscope (SEM) equipped with a field emission gun (FEG) and coupled with an energy dispersive X-ray spectrometer (EDX) operating at an accelerating voltage of 15 kV. Chemical phases identification was done by X-ray diffraction (XRD) using a Bruker D8-A25 diffractometer with Cu Kα (λ = 0.154056 nm), a step of 0.02° and a scan rate of 1.8 seconds per step.

The typical morphologies of samples elaborated by HIP and PTAW are shown in Figure 1. The HIPed Norem02 (Figure 1 (a)) presents a fine-grained microstructure. XRD coupled with SEM-EDX analyses performed in previous studies [21-22] revealed that the matrix is primarily austenitic and only contains a small amount of ferrite. Small $M_{23}C_6$-type carbides (M = Cr, Mn, Mo) are homogeneously dispersed in the matrix: globular carbides in zones between the primary powder particles and lath-like interdendritic carbides inside the particles (see supplementary material S1). On the other hand, as shown by XRD and SEM-EDX analyses (see supplementary materials S2 and S3), the Norem02 elaborated by PTAW (Figure 1(b)) is composed of large austenitic grains, a small amount of ferrite, acicular intergranular M_7C_3-type carbides (see supplementary material S4) and intergranular Si and Mo enriched phases. Table I reports the mechanical properties of the HIPed Norem02 and of the alloy elaborated by PTAW. Tensile tests were performed on flat specimens machined in the HIPed part to determine the Young's modulus, the yield and ultimate tensile strengths and the fracture elongation. Properties of the PTAW alloy were found in ref. [23]. The hardness of

both samples was measured in Vickers configuration under a load of 500 g (4.9 N). It is worth noting that the HIPed Norem02 presents superior mechanical properties than the one elaborated by PTAW.

Wear tests were performed at room temperature using a pin-on-disk tribometer (Anton-Paar Instruments) in a ball-on-plate configuration under different normal loads (2, 5 and 10 N) against a WC-Co ball counterpart (6 mm diameter). These parameters are based on a previous work of Liu *et al.* [24]. However, in the present study, the linear velocity (0.05 $m \cdot s^{-1}$) was about three times higher than in ref. [24]. The total sliding distance was 100 m. Moreover, WC-Co (instead of the 100C6 steel, for instance, or Si_3N_4 used in ref. [24]) was selected as counterpart because it is a carbide (as the hard phases present in the Norem02) and has high mechanical properties (nominal hardness of 1570 HV and Young modulus of 610 GPa), higher than that of the Norem02 (Table I). The wear of the ball was consequently avoided. The WC-Co ball is grade 10, following the ABMA norm, with a roughness of 25 nm. The surface arithmetical roughness Sa of Norem02 elaborated by HIP and PTAW is 15 and 50 nm, respectively.

For each load, a rotation radius of 1.5, 2.5 and 3.5 mm was used, keeping constant the linear speed and the total friction length. It allowed verifying that the rotation radius does not influence neither the shape and size of the wear track, nor the value of the friction coefficient. Friction force-distance curves were obtained for each applied load. For each curve, zones where the friction force is constant (plateau) were identified. The corresponding mean tangential forces were plotted versus the three normal loads in order to determine the friction coefficient, which is the slope of the line according to the Coulomb's friction law. For each elaboration process (HIP and PTAW), nine measurements were performed (the three loads were applied on three rotation radii) on the different samples to estimate the friction coefficient, in order to assess the repeatability.

After tribological tests, wear tracks were observed by a 3D optical profiler (WYKO NT1100). Surface maps were obtained and the depths and widths of the worn areas were measured using Gwyddion software [25]. For each track, four zones were chosen in four orthogonal directions and one depth profile per zone was measured. The depth and width of the wear track were finally calculated as the average of the values measured in the four zones. Two samples at a given condition were considered to calculate the mean depth and width of each wear track. In addition, for each measured zone, Gwyddion software calculates the worn area (area of the curve below the initial surface), making it possible to estimate the volume and the weight losses and to calculate the wear rate.

Finally, wear tracks (surfaces and cross-sections) were characterised by SEM-EDX, using the apparatus described above. In the case of the cross sections, only wear tracks obtained under a load of 10 N are presented, as the differences between the two samples are more significant under this load.

3. Results and discussion

3.1 Optical profiler characterisations of wear tracks

Figure 2 shows the 3D surface maps of the tracks after wear tests under the three loads. Figure 3 presents the corresponding 2D profiles. Under a load of 2 N, for both samples (HIP and PTAW), it is possible to observe a partial material redeposition on the edges of the tracks, causing the formation of a relief with a height ranging between 0.5 and 1 µm in the case of the HIPed Norem02 (Figure 2 (a)) and between 1 and 2 µm for the alloy elaborated by PTAW (Figure 2 (b)). The wear track of the sample elaborated by PTAW appears wider and more damaged than the one formed in the case of the HIPed alloy. The depth of the wear track ranges between 0.5 and 1 µm in the case of the HIPed sample and has an average value of 1 µm for the Norem02 obtained by PTAW.

Under a load of 5 N, the average depth of the wear track is about 1 µm for the HIPed sample (Figure 2 (c)) and 3 µm for the Norem02 elaborated by PTAW (Figure 2 (d)). For the latter, some areas present an increased depth, ranging between 4 and 5 µm, with some localised zones exceeding 6 µm. A redeposition of material on the edges of the track occurred for both samples during the wear test, as observed under 2 N.

The differences in the depths of the wear tracks when passing from a load of 2 to 5 N, are more significant for the Norem02 elaborated by PTAW than for the HIPed sample.

Finally, under a load of 10 N, the mean depth is about 2.5 µm for the HIPed sample (Figure 2 (e)). In the case of the alloy elaborated by PTAW (Figure 2 (f)), the wear track is formed by parallel grooves and presents a mean depth ranging between 6 and 7 µm with a maximum of 10 µm. As previously observed, the differences in the depth of the worn surfaces when passing from a load of 5 N to 10 N are more significant for the sample elaborated by PTAW.

Concerning the width of the wear tracks, a constant difference of around 115 µm between the HIPed sample and the alloy elaborated by PTAW is observed and seems to be independent on the applied load.

These results indicate that the elaboration by HIP improves the wear resistance of the Norem02 at room temperature. The reason of this behaviour is explained in terms of microstructure. As shown in Figure 1, the average grain size of the HIPed hardfacing is smaller than in the PTAW one. Moreover, it is known that the wear resistance of a material is increased by the presence of hard phases, such as carbides [11-17]. As reported by Karlsson [26], the distribution of the carbides plays a major role in wear behaviour. A homogeneous distribution, as in the case of the HIPed sample where carbides are located inside the austenitic grains and between the primary powder particles, will improve the resistance against the surface deterioration. On the contrary, in the case of the alloy elaborated by PTAW, carbides and Si-Mo enriched phases are located in the intergranular zones, leaving large austenitic matrix areas exposed to wear phenomenon.

3.2 Estimation of wear rates and friction coefficients.

The wear rate estimated for each sample under the different tested conditions are presented in Figure 4. The wear rates calculated after wear tests under 2 N are similar for the samples elaborate by HIP ($(8.1 \pm 1.6)\cdot10^{-6}$ mm^3.m^{-1}) and PTAW ($(7.8 \pm 1.6)\cdot10^{-6}$ mm^3.m^{-1}). The difference becomes significant at higher load: at 5 N, the wear rate of the alloy increased to $(24 \pm 5)\cdot10^{-6}$ mm^3.m^{-1} and $(79 \pm 16)\cdot10^{-6}$ mm^3.m^{-1} for the samples elaborate by HIP and PTAW respectively; at 10 N, the wear rate of the alloy increased again to $(86 \pm 17)\cdot10^{-6}$ mm^3.m^{-1} and $(440 \pm 90)\cdot10^{-6}$ mm^3.m^{-1} for the samples elaborate by HIP and PTAW respectively. At 10 N, the wear rate of the HIPed alloy is close to the values estimated for the sample elaborated by PTAW, but under a load of 5 N. Generally, the wear rate increases with the applied load, but the increase is more significant for the sample elaborated by PTAW. In the case of the HIPed Norem02, the wear rate is multiplied by a factor 10 between 2 N and 10 N, while for the alloy elaborated by PTAW, the difference is of two orders of magnitude.

Even if no work on Norem02 performed in the experimental conditions used in the present study exists in the literature, it is still possible to consider, for comparison, the results reported by Bourithis *et al.* [13]. The authors tested the wear behaviour of a tool steel containing 1.5 wt. % of carbon. After wear tests of a total length of about 1050 m, under an applied load of 9.8 N and a linear speed ranging from 0.05 m.s^{-1} to 0.75 m.s^{-1}, they found wear rates varying between $4\cdot10^{-3}$ and $1.6\cdot10^{-2}$ mm^3.m^{-1}. Considering the shorter sliding distance in the present study, the Norem02 wear rates are consistent with these typical values measured for reference steels in the field of wear resistance.

Friction force-distance curves obtained under different loads (Figure 5) allowed calculating the friction coefficients. This parameter corresponds to the slope of the regression line

obtained plotting the mean friction force measured as a function of the normal load [27] (Figure 5 insets). The advantage of this statistical method is to avoid the problems due to the dispersion of a single measurement. It is interesting to note that, for both HIPed and PTAW samples, friction force-distance curves display the existence of three distinct friction behaviours for all tested loads (Figure 5). The first behaviour corresponds to the running-in period from the start of the test and for few sliding meters. This stage is characterized by a low friction coefficient (0.12 and 0.18 for the HIPed and PTAW hardfacing respectively) and ends with a sharp increase of the friction force. The following behaviour is a quasi-stable regime, where the friction force signal is highly serrated. For both samples, the friction coefficients are equal to 0.39. This first plateau progressively increases to the last behaviour characterized by a higher friction coefficient (0.57 and 0.74 for the HIPed and PTAW hardfacing respectively) and a more stable friction force, except local variations. During the running-in period, the WC-Co ball slides on the micro asperities of the surface, i.e. the hard carbides phases. For the PTAW, the large austenitic grains lead to more adhesive contact and consequently a higher friction coefficient. This period ends with the formation of the third body composed of carbides and austenite debris. In the first plateau, abrasive wear is the dominant mechanism. The progressive transition from the first plateau to the second one can be explained by the increase of the temperature during friction and the formation of an oxide layer protecting the Norem02 from further abrasion. The friction is mainly dominated by adhesive mechanisms characterized by the higher friction coefficient and occasional removal of the transfer layer. The higher friction coefficient (0.74 compared to 0.57) of the PTAW alloy comes from the largest contact surface, as observed by profilometry. Generally, a high friction coefficient is associated to an intensive friction, leading to major damages. Persson *et al*. [3] evaluated friction and galling properties of laser processed Norem02 using load-scanning tests. They associate the increase of the friction coefficient to massive galling occurring at high temperature and probably due to the absence of strain-induced martensitic

transformation. They reported that at elevated temperatures (> 250 °C) the friction coefficient of the laser processed Norem02 reaches 0.5-0.7 and the predominant wear mechanism becomes adhesive wear. In the present study, the friction coefficient of the HIPed Norem02 calculated considering the second plateau, can be associated to less severe friction, leading to less important surface degradation, than the one obtained for the alloy elaborated by PTAW.

It is worth noting that the transition from the first to the second friction plateau is delayed with the increase of the load. This can be explained by the removal of the oxide layer due to the presence of abrasive particles, which amount increases with the normal load and the wear or the hardfacing. This delay is systematically longer for the PTAW alloy and the second plateau is even not attained under a load of 10 N after 100 m. This is in agreement with the wear rate and the surface maps and depth profiles results, showing that the microstructure obtained by HIP allows the material to better withstand mechanical stress during friction tests. It is important to underline that tribological tests were realised at room temperature. A trend reversal, with a modification of the wear mechanisms, cannot be excluded at more elevated temperatures.

3.3 MEB-EDX analyses of wear tracks.

In order to confirm the wear mechanisms of the sample elaborated by HIP, the worn surfaces obtained under different loads at the end of the friction tests were analysed by SEM-EDX. Figure 6 shows the SEM micrographs of the surface of the wear track after the test under a load of 2 N. The track is composed of grooves originating from the abrasive wear of the first plateau and covered by a non-continuous transfer layer. EDX analyses reveal that this layer is composed of oxides, rich in Cr and Fe (see supplementary material S5), confirming the occurrence of oxidative wear in a second time. Grooves are also visible above the oxide layer. They are generally associated to abrasive wear [26] but they also can form from plastic deformation [13]. Figure 6 (b) displays a magnification of an area containing oxides. Close to

the zones where the oxide layer was fractured and removed, it is possible to note the presence of tongue-shaped area, all having the same direction and indicating the displacement direction of the second body during the wear test. This kind of morphology is commonly associated to adhesive wear [28]. The worn track presents typical marks of abrasive wear followed by oxidative but also adhesive ones.

The worn track obtained under a load of 5 N is displayed in Figure 7. Again, large grooves covered by an oxide layer (see supplementary material S6) can be observed. The grooves are deeper than those formed under 2 N. Some cavities can also be noticed, which result from the removal of debris off the metallic matrix. Unfortunately, the nature of the debris could not be determined. The magnification (Figure 7 (b)) shows a zone where the oxide layer was fractured and partially removed; some tongue-shaped area, associated to an adhesive wear mechanism, were also revealed. As previously suggested, abrasive followed by both oxidative and adhesive mechanisms are involved in the sample wear. As reported by Bourithis *et al*. [13], the presence of cavities and deep grooves indicates that oxidation is not the primary wear mechanism.

The surface of the worn track obtained under 10 N is presented in Figure 8. As revealed for lower loads, oxides are present and grooves are clearly visible. Some cavities can be noticed, as observed under 5 N. The oxide layer seems more discontinuous. Tongue-shaped area are more numerous and are larger than those observed under 2 and 5 N (Figure 8 (b)). EDX analyses revealed the presence of Cr and Fe enriched oxides inside some tongue-shaped area (see supplementary material S7). This might be the result of trapping of the oxides during the tongue-shaped area formation or a consequence of the redeposition phenomenon. These results confirm that oxidative and adhesive wear contribute to the global wear mechanism after the abrasive period.

Some authors report the formation of strain-induced martensite, generally below 180 °C [4, 29]. In the present study, XRD analyses of the worn track after the test under 10 N were

performed but the presence of martensite was not revealed. On one hand, the conditions leading to the formation of strain-induced martensite might have been modified by the elaboration by HIP; on the other hand, it is also possible that the stress induced by an applied load of 10 N is not sufficient to trigger the strain-induced martensitic transformations.

The cross-section of the HIPed sample after tests under 10 N was also characterised by SEM-EDX near the middle of the wear track (Figure 9). The sample surface appears plastically deformed; no cracks are visible close to the surface or more deeply in the bulk. In agreement with the previous characterisations, the presence of Cr and Fe enriched oxides was revealed at the surface of the wear track by EDX analyses; no oxide was detected below the surface.

In order to compare the two elaboration processes, a global view of the cross-section of the worn track of the Norem02 elaborated by PTAW after wear test under 10 N is shown in Figure 10 (a). The friction force-distance curve shows that the second friction plateau, mainly dominated by oxidation and adhesive wear, was not reached under this load. A deformation of the sample surface can be observed, as well as grooves. No cracks are visible close to the surface or into the bulk. The magnification (Figure 10 (b)) confirms that the sample is damaged only close to the surface, where a significant plastic deformation occurred. This deformation leaded to a modification of the morphology of the carbides located close to the surface, which became more globular. Locally, a wear debris accumulation was revealed, as well as the presence of some spalled zones. EDX analyses indicated that these debris are mainly a mixture of Cr and Fe enriched oxides; some particles present a high amount of carbon and were identified as carbides. Figure 11 shows that debris are either incorporated in the spalled areas (zone 1) or accumulated at the surface (zone 2). The presence of the debris can be associated to abrasive wear [30, 31], supporting the results obtained by the friction force-distance curve under this load. Furthermore, these debris certainly participated to the abrasive wear mechanism, acting as a third body formed by phases harder than the metallic matrix (such as oxides or carbides) [32].

These results prove that, also in the case of the sample elaborated by PTAW, oxidation occurred, as it was observed for the HIPed alloy, but the increased stress during the wear test caused the pull-out of the oxides and of the material itself.

4. Conclusions

The tribological properties of a Fe-based hardfacing alloy Norem02 elaborated by HIP was investigated and compared to the performance of the same material elaborated by PTAW, a more conventional hardfacing technique. The main findings can be summarized as follow:

- Under loads higher than 2 N, the HIPed Norem02 presents a better wear resistance than the alloy elaborated by PTAW. Wear tracks of HIPed alloy are less deep and wide. The wear rates estimated for the HIPed Norem02 are lower (under a load of 10 N, the difference in wear rates between the two materials is about 5.5 times).
- Three friction coefficients were calculated for the Norem02 elaborated by HIP and by PTAW, considering the running-in period and the two plateaus of the friction force-distance curves. The friction coefficient of the HIPed Norem02 calculated considering the second plateau is significantly lower compared to the sample elaborated by PTAW.
- MEB-EDX analyses revealed typical marks of oxidative and adhesive wear covering the deep grooves of the initial abrasive wear and confirming that two mechanisms are involved in the wear. Firstly, a dominance of abrasive wear, secondly a dominance of oxidative and adhesive wear.
- These performances confirm that the elaboration by HIP is a promising way to improve the tribological behaviour of Norem02 as hardfacing, thanks to the fine microstructure obtained, shortening the duration and reducing the effect of the abrasive wear period compared to the sample elaborated by PTAW.

Acknowledgements

The authors would like to thank the Bourgogne-Franche-Comté Region for financing part of this study and Framatome, which finances the Chair in which this program is included.

References

[1] S. Pawar, A. K. Jha, G. Mukhopadhyay, Effect of different carbides on the wear resistance of Fe-based hardfacing alloys, Int. J. Refract. Met. Hard Mater. 78 (2019) 288-295. https://doi.org/10.1016/j.ijrmhm.2018.10.014

[2] H. Ocken, The galling wear resistance of new iron-base hardfacing alloys: a comparison with established cobalt- and nickel-base alloys, Surf. Coat. Tech. 76-77 (1995) 456-461. https://doi.org/10.1016/0257-8972(95)02573-1

[3] D. E. Persson, S. Jacobson, S. Hogmark, Effect of temperature on friction and galling of laser processed Norem02 and Stellite 21, Wear 255 (2003) 498-503. https://doi.org/10.1016/S0043-1648(03)00122-4

[4] J.-K. Kim, S.-J. Kim, The temperature dependence of the wear resistance of iron-base NOREM 02 hardfacing alloy, Wear 237 (2000) 217-222. https://doi.org/10.1016/S0043-1648(99)00326-9

[5] H. Ocken, Reducing the Cobalt Inventory in Light Water Reactors, Nucl. Technol. 68 (1995) 18-28. https://doi.org/10.13182/NT85-A33563

[6] N.-R. Park, D. G. Ahn, Wear characteristics of Stellite6 and NOREM02 hardfaced SKD61 hot working tool steel at the elevated temperature, Int. J. Precis. Eng. Manuf. 15 (2014) 2549-2558. https://doi.org/10.1007/s12541-014-0626-0

[7] E. K. Ohriner, T. Wada, E. P. Whelan, H. Ocken, The chemistry and structure of wear resistant, iron-base hardfacing alloys, Metall. Trans. A 22A (1991) 983-991. https://doi.org/10.1007/BF02661091

[8] S. Vaidya, S. Mahajan, C. M. Preece, The role of twinning in the cavitation erosion of cobalt single crystals, Metall. Trans. 11A (1980) 1139-1150. https://doi.org/10.1007/BF02668138

[9] K. J. Bhansal, A. E. Miller, The role of stacking fault energy on galling and wear behaviour, Wear 75 (1982) 241-252. https://doi.org/10.1016/0043-1648(82)90151-X

[10] J. Vikström, Galling resistance of hardfacing alloys replacing Stellite, Wear 179 (1994) 143-146. https://doi.org/10.1016/0043-1648(94)90232-1

[11] L. Xu, W. Song, S. Ma, Y. Zhou, K. Pan, S. Wei, Effect of slippage rate on frictional wear behaviors of high-speed steel with dual-scale tungsten carbides (M_6C) under high-pressure sliding-rolling condition, Tribol. Int. 154 (2021) 106719. https://doi.org/10.1016/j.triboint.2020.106719

[12] A. S. Chaus, M. Sahul, R. Moravčík, R. Sobota, Role of microstructural factor in wear resistance and cutting performance of high-speed steel end mills, Wear 474-475 (2021) 203864. https://doi.org/10.1016/j.wear.2021.203865

[13] L. Bourithis, G. D. Papadimitriou, J. Sideris, Comparison of wear properties of tool steels AISI D2 and O1 with the same hardness, Tribol. Int. 39 (2006) 479-489.

[14] D. N. Korade, K. V. Ramana, K. R. Jagtap, Study of effect of population density of carbides on surface roughness and wear rate of H21 tool steel, Mater. Today Proc. 19 (2019) 228-232. https://doi.org/10.1016/j.matpr.2019.06.709
[15] E. Iakovakis, M. J. Roy, M. Gee, A. Matthews, Evaluation of wear mechanisms in additive manufactured carbide-rich tool steels, Wear 462-463 (2020) 203449. https://doi.org/10.1016/j.wear.2020.203449

[16] P. Karlsson, P. Krakhmalev, A. Gåård, J. Bergström, Influence of work material proof stress and tool steel microstructure on galling initiation and critical contact pressure, Tribol. Int. 60 (2013) 104-110. https://doi.org/10.1016/j.triboint.2012.10.023

[17] P. Karlsson, A. Gåård, P. Krakhmalev, Influence of tool steel microstructure on friction and initial material transfer, Wear 319 (2014) 12-18.
https://doi.org/10.1016/j.wear.2014.07.002

[18] N. Ur Rahman, M. B. de Rooij, D. T. A. Matthews, G. Walmag, M. Sinnaeve, G. R. B. E. Römer, Wear characterization of multilayer laser cladded high speed steels, Wear 130 (2019) 52-62. https://doi.org/10.1016/j.tribo int.2018.08.019

[19] U. Malayoglu, A. Neville, Comparing the performance of HIPed and Cast Stellite 6 alloy in liquid–solid slurries, Wear 255 (2003) 181-194. https://doi.org/10.1016/S0043-1648(03)00287-4

[20] M. Wong Kian, L. A. Cornish, A. van Bennekom, Comparison of erosion–corrosion behaviour of hot iso statically pressed and welded Stellite coatings, J. S. Afr. Inst. Min. Metall. 95 (1995) 319-335. https://hdl.handle.net/10520/AJA0038223X_2313

[21] A. Tellier, M. R. Ardigo-Besnard, J.-P. Chateau-Cornu, Influence of the process parameters on the microstructure of a hardfacing coating elaborated by Hot Isostatic Pressing, Arch. Metall. Mat. 64 (2019) 33-38. https://doi.org/10.24425/amm.2019.126215

[22] A. Tellier, M. R. Ardigo-Besnard, J.-P. Chateau-Cornu, R. Chassagnon, J.-M. Fiornai, Characterization of the interfacial zone between a HIPed Fe-based alloy and a stainless steel container, J. Mater. Eng. Perform. 29 (2020) 3800-3811. https://doi.org/10.1007/s11665-020-04897-5

[23] G. Beaurin, J.-P. Mathieu, E. Gauthier, D. Nelias, M. Coret, F. Arnoldi, Microstructural and mechanical properties evolutions of plasma transferred arc deposited Norem02 hardfacing alloy at high temperature, Mater. Sci. and Eng. A 528 (2011) 5096-5105. https://doi.org/10.1016/j.msea.2011.02.077

[24] X.-B. Liu, G.-Y. Fu, S. Liu, S.-H. Shi, X.-M. He, M.-D. Wang, High temperature wear and corrosion resistance of Co-free Ni-based alloy coatings on nuclear valve sealing surfaces, Nuc. Eng. Design 241 (2011) 4924-4928. https://doi.org/10.1016/j.nucengdes.2011.09.021

[25] http://gwyddion.net/

[26] P. Karlsson, A. Gåård, P. Krakhmalev, J. Bergström, Galling resistance and wear mechanisms for cold-work tool steels in lubricated sliding against high strength stainless steel sheets, Wear 286–287 (2012) 92-97. https://doi.org/10.1016/j.wear.2011.04.002

[27] P. Stempflé, F. Pollet, L. Carpentier, Influence of intergranular metallic nanoparticles on the fretting wear mechanisms of Fe- Cr- Al2O3 nanocomposites rubbing on Ti- 6Al- 4V, Trib. Inter. 41 (2008) 1009-1019. https://doi.org/10.1016/j.triboint.2008.02.019

[28] J.-N. Aoh, Y.-R. Jeng, E.-L. Chu, L.-T. Wu, On the wear behavior of surface clad layers under high temperature, Wear 225-229 (1999) 1114-1122. https://doi.org/10.1016/S0043-1648(98)00393-7

[29] K.-Y. Lee, G. G. Kim, J. H. Kim, S.-H. Lee, S.-J. Kim, Sliding wear behavior of hardfacing alloys in a pressurized water environment, Wear 262 (2007) 845-849. https://doi.org/10.1016/j.wear.2006.08.015

[30] K.-H. Zum Gahr, Microstructure and wear of materials, first ed. Elsevier, North Holland, 1987.

[31] A. Dalmau, W. Rmili, D. Joly, C. Richard, A. Igual-Muñoz, Tribological Behavior of New Martensitic Stainless Steels Using Scratch and Dry Wear Test, Tribol. Lett. 56 (2014) 517-529. https://doi.org/10.1007/s11249-014-0429-6

[32] J. Denape, Third body concept and wear particle behavior in dry friction sliding conditions. Key Eng. Mater. 640 (2015) 1-12. https://doi.org/10.4028/www.scientific.net/KEM.640.1

Tables

Table I: mechanical properties of Norem02 elaborated by HIP and PTAW at room temperature.

	HIP (present study)	**PTAW**
Young's modulus (GPa)	227	187 [23]
Ultimate tensile strength (MPa)	1177	867 [23]
Yield strength (MPa)	840	621 [23]
Fracture elongation (%)	3.2	1.4 [23]
Hardness (HV0.5)	471 ± 24	413 ± 18

Figure captions

Figure 1: SEM images of Norem02 elaborated by (a) HIP and (b) PTAW.

Figure 2 : Surface maps of Norem02 after wear tests with a load of 2 N (a) HIP and (b) PTAW; with a load of 5 N (c) HIP and (d) PTAW; with a load of 10 N (e) HIP and (f) PTAW.

Figure 3: 2D depth profiles under different loads for the Norem 02 elaborated by (a) HIP and (b) PTAW.

Figure 4: Wear rates under different loads for the Norem 02 elaborated by HIP (white bar) and PTAW (grey bar).

Figure 5: Friction force-distance curves under different loads obtained for the (a) HIPed sample and (b) the alloy elaborated by PTAW. Insets: tangential force function of the normal force for the running-in period of the friction force-distance curves (black triangles), the first friction plateau (grey circles) and the second one (white squares).

Figure 6: SEM micrographs of the surface of the wear track of the HIPed sample under 2 N, (a) global view and (b) magnification of a zone containing oxides.

Figure 7: SEM micrographs of the surface of the wear track of the HIPed sample under 5 N, (a) global view and (b) magnification of a zone containing oxides.

Figure 8: SEM micrographs of the surface of the wear track of the HIPed sample under 10 N, (a) global view and (b) magnification of a zone containing tongue-shaped area and oxides.

Figure 9: SEM micrographs of the cross-section of the HIPed sample after test under 10 N.

Figure 10: SEM micrographs of the cross-section of the worn track of Norem02 elaborated by PTAW after test under 10 N, (a) global view and (b) magnification.

Figure 11: Cross-section of the worn track of Norem02 elaborated by PTAW. Zone 1: debris incorporated in a spalled area; zone 2: oxides debris.

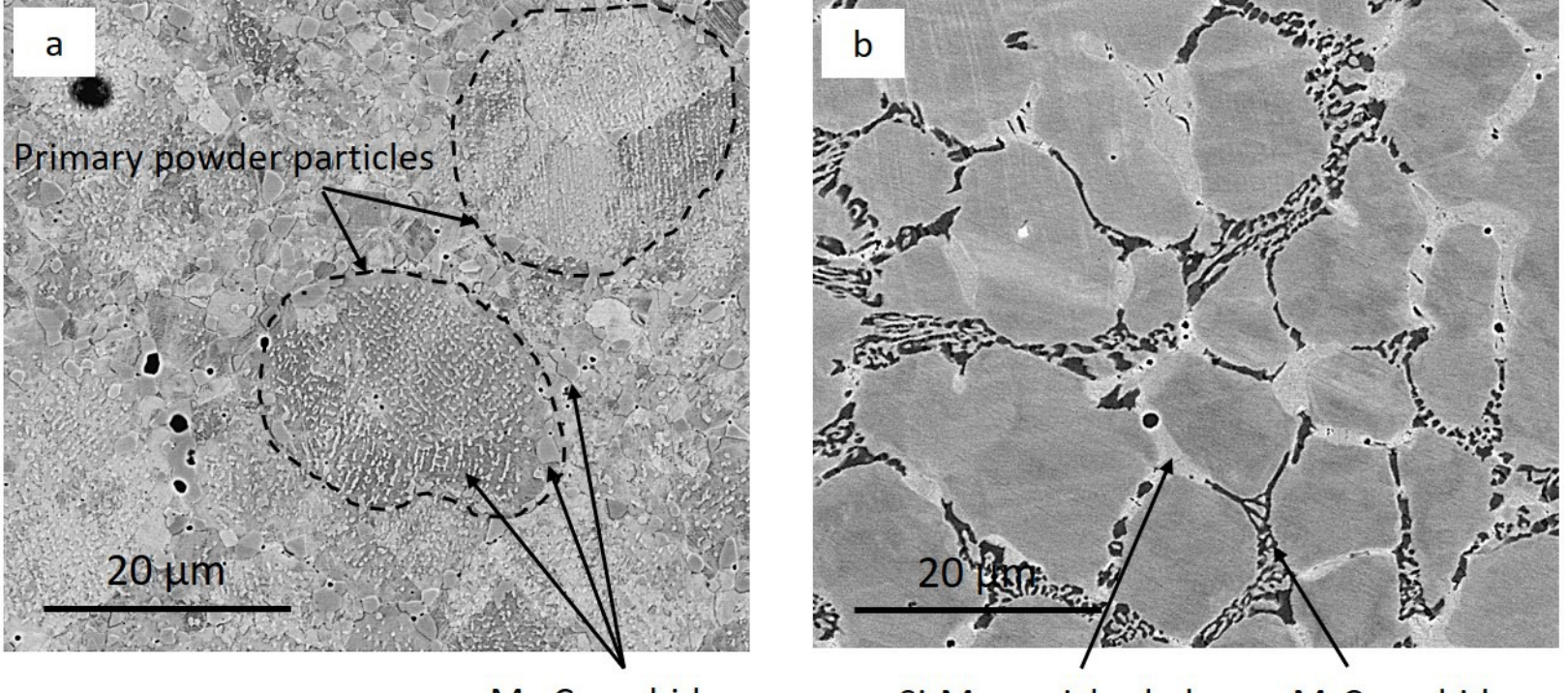
a
Primary powder particles
20 µm
$M_{23}C_6$ carbides
b
20 µm
Si-Mo enriched phase
M_7C_3 carbides

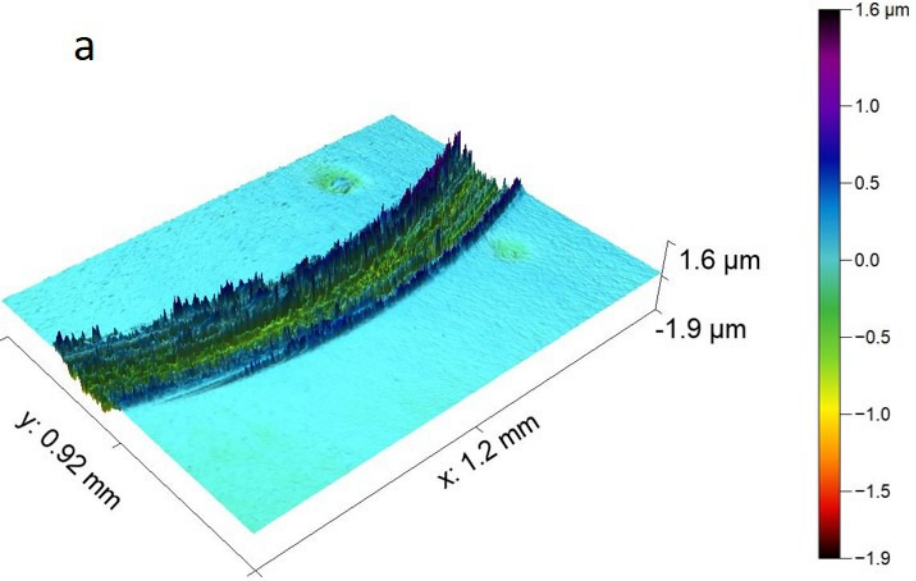
a
1.6 µm
-1.9 µm
y: 0.92 mm
x: 1.2 mm
1.6 µm
1.0
0.5
0.0
−0.5
−1.0
−1.5
−1.9

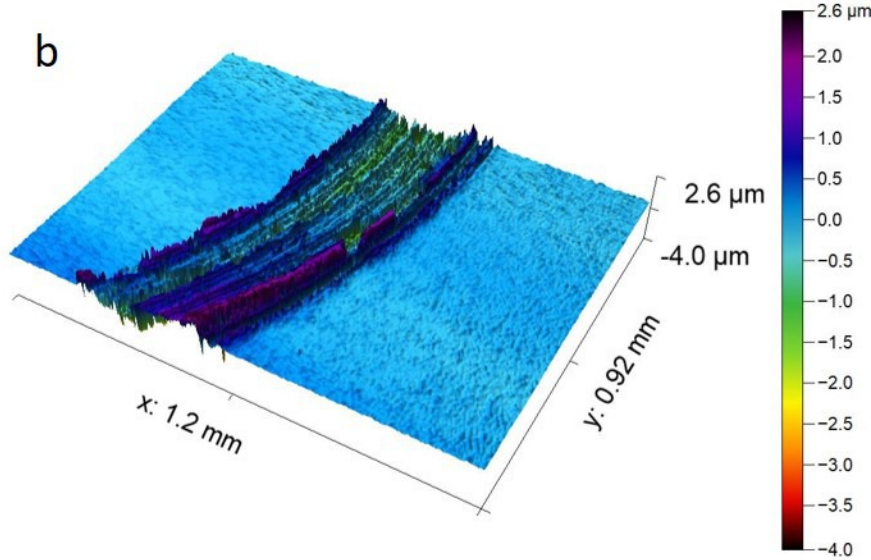
b
2.6 µm
-4.0 µm
x: 1.2 mm
y: 0.92 mm
2.6 µm
2.0
1.5
1.0
0.5
0.0
−0.5
−1.0
−1.5
−2.0
−2.5
−3.0
−3.5
−4.0

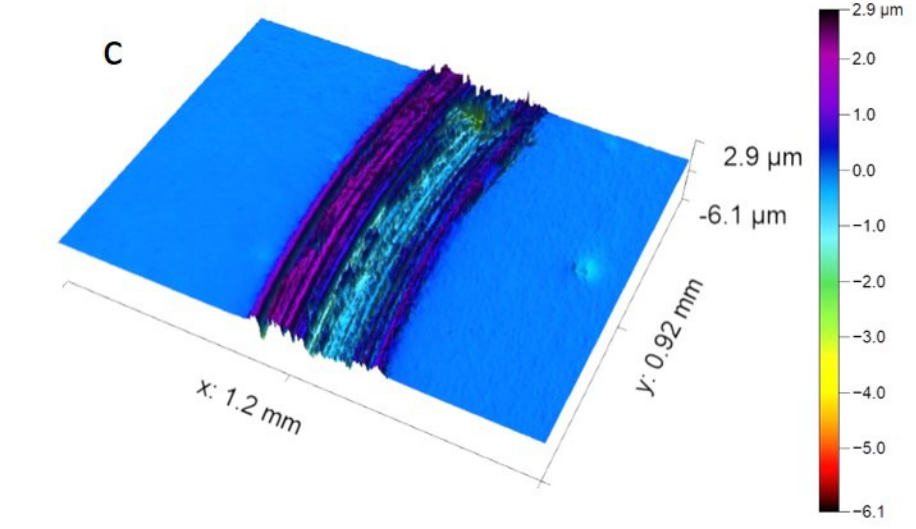
c
2.9 µm
-6.1 µm
x: 1.2 mm
y: 0.92 mm
2.9 µm
2.0
1.0
0.0
−1.0
−2.0
−3.0
−4.0
−5.0
−6.1

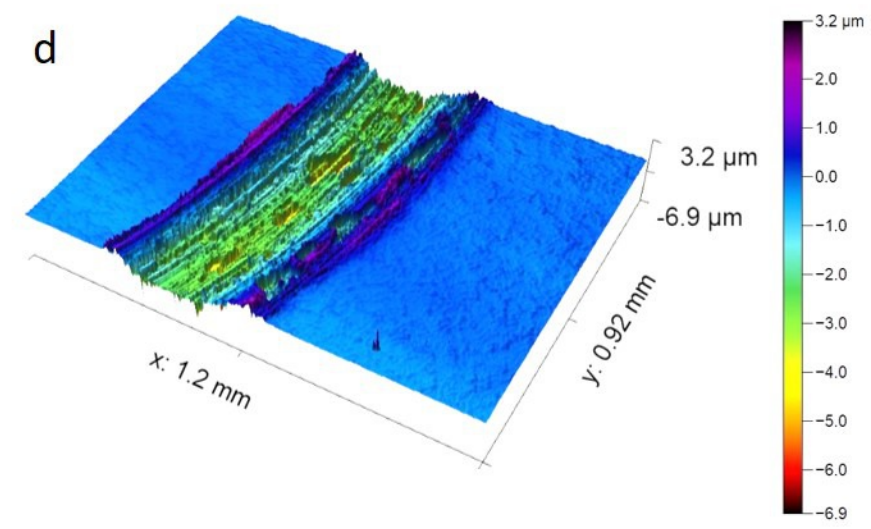
d
3.2 µm
-6.9 µm
x: 1.2 mm
y: 0.92 mm
3.2 µm
2.0
1.0
0.0
−1.0
−2.0
−3.0
−4.0
−5.0
−6.0
−6.9

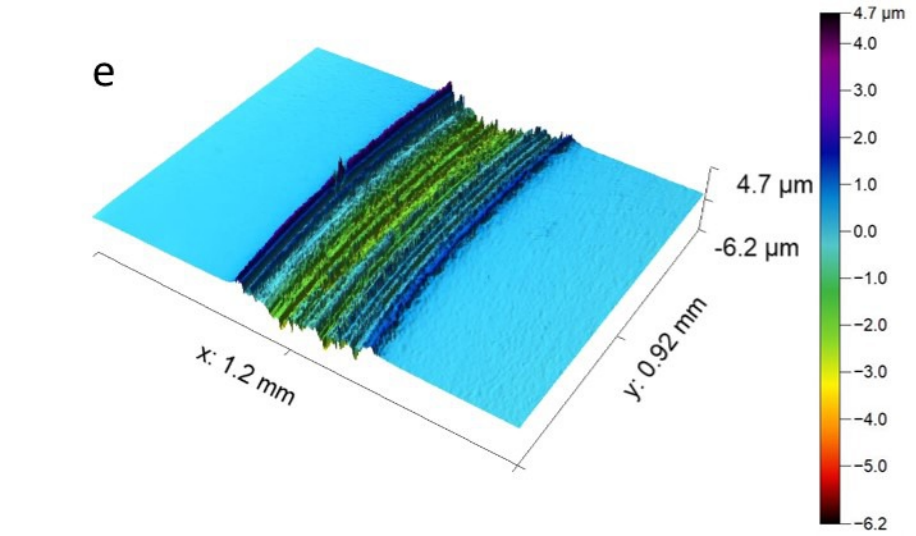
e
4.7 µm
-6.2 µm
x: 1.2 mm
y: 0.92 mm
4.7 µm
4.0
3.0
2.0
1.0
0.0
−1.0
−2.0
−3.0
−4.0
−5.0
−6.2

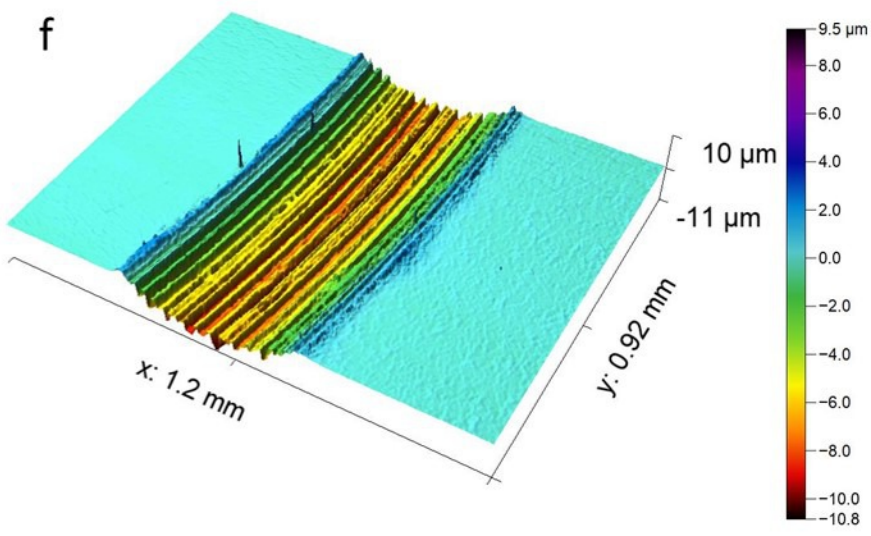
f
10 µm
-11 µm
x: 1.2 mm
y: 0.92 mm
9.5 µm
8.0
6.0
4.0
2.0
0.0
−2.0
−4.0
−6.0
−8.0
−10.0
−10.8

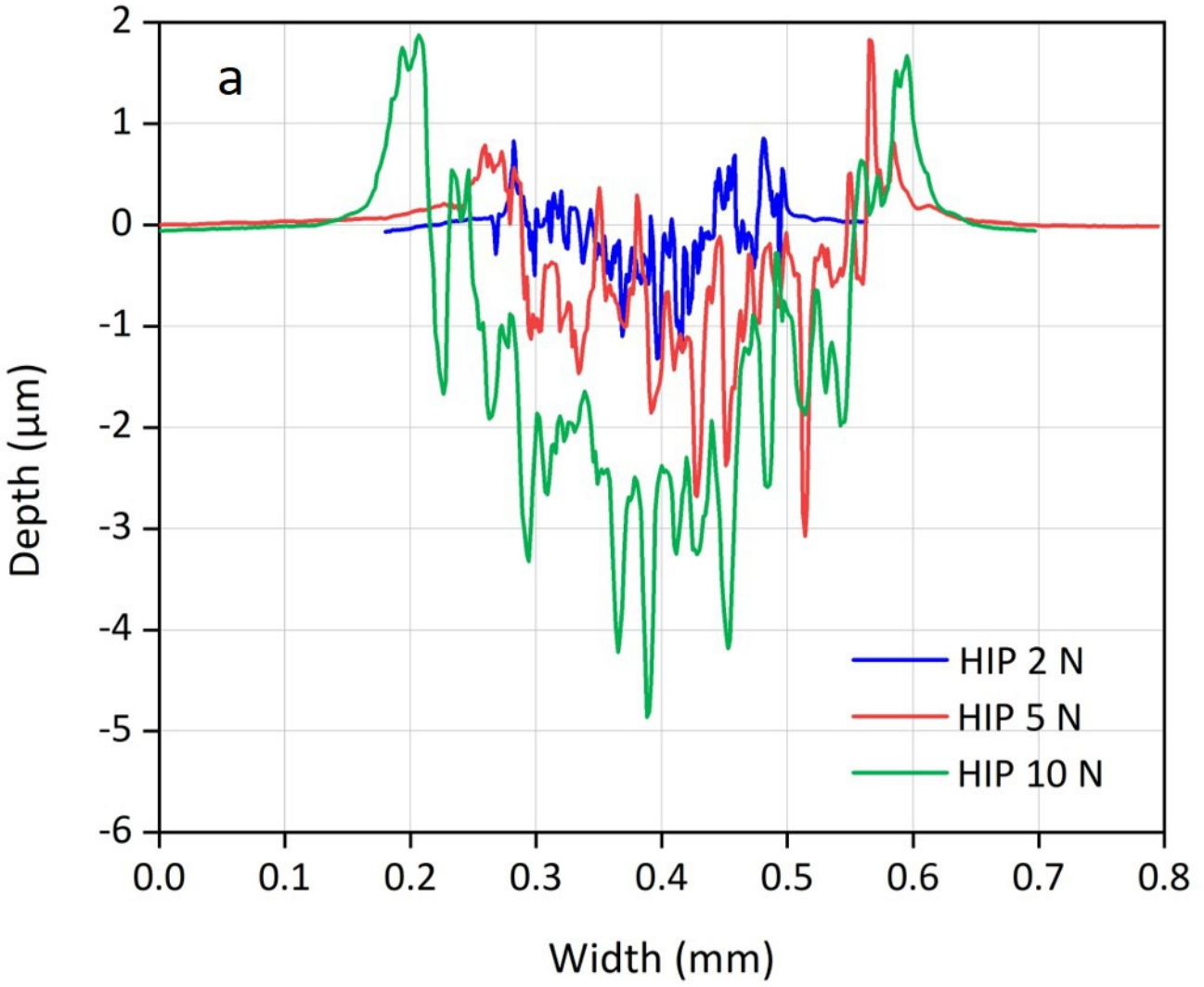
a
Depth (µm)
Width (mm)
HIP 2 N
HIP 5 N
HIP 10 N

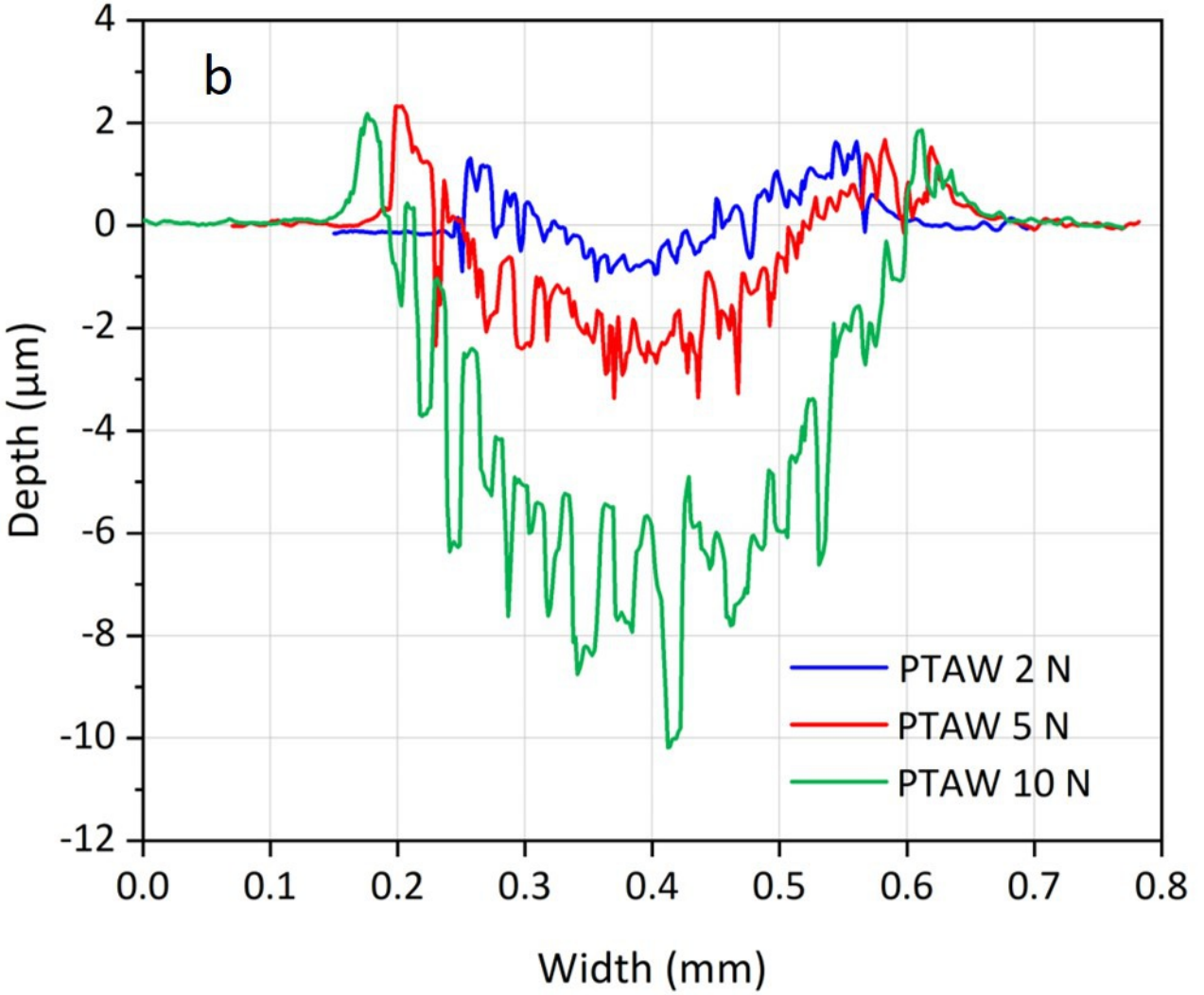
b
Depth (µm)
Width (mm)
PTAW 2 N
PTAW 5 N
PTAW 10 N

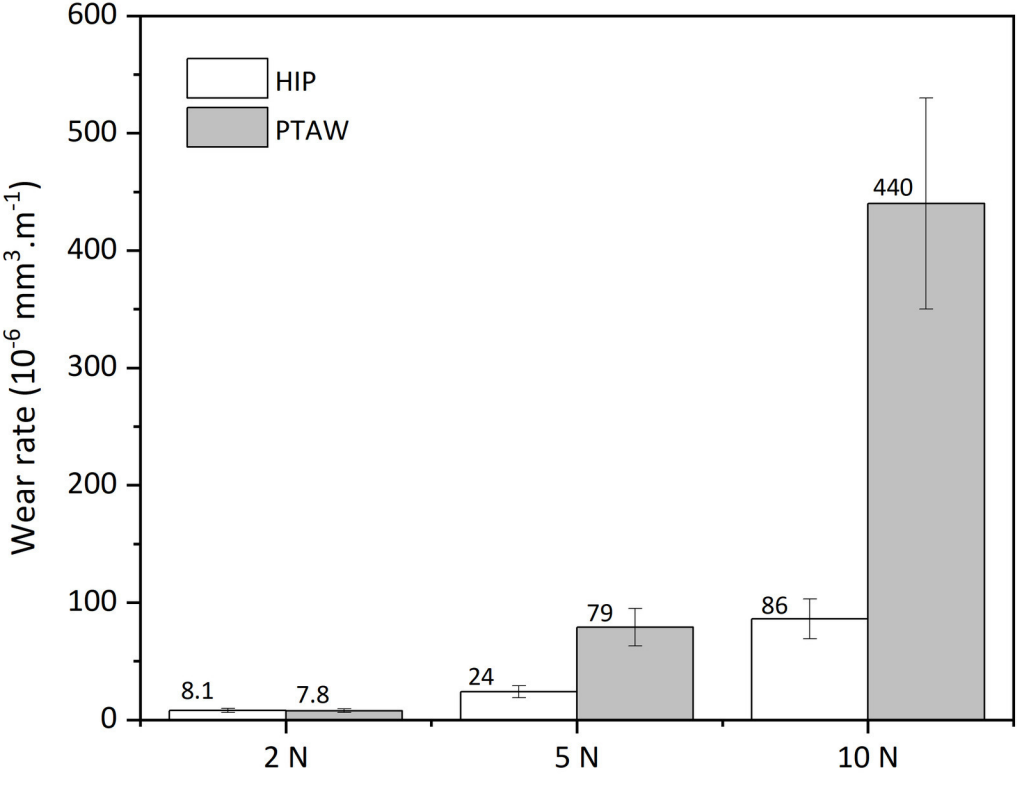
HIP
PTAW
Wear rate (10^{-6} $mm^3.m^{-1}$)
600
500
400
300
200
100
0
8.1
7.8
24
79
86
440
2 N
5 N
10 N

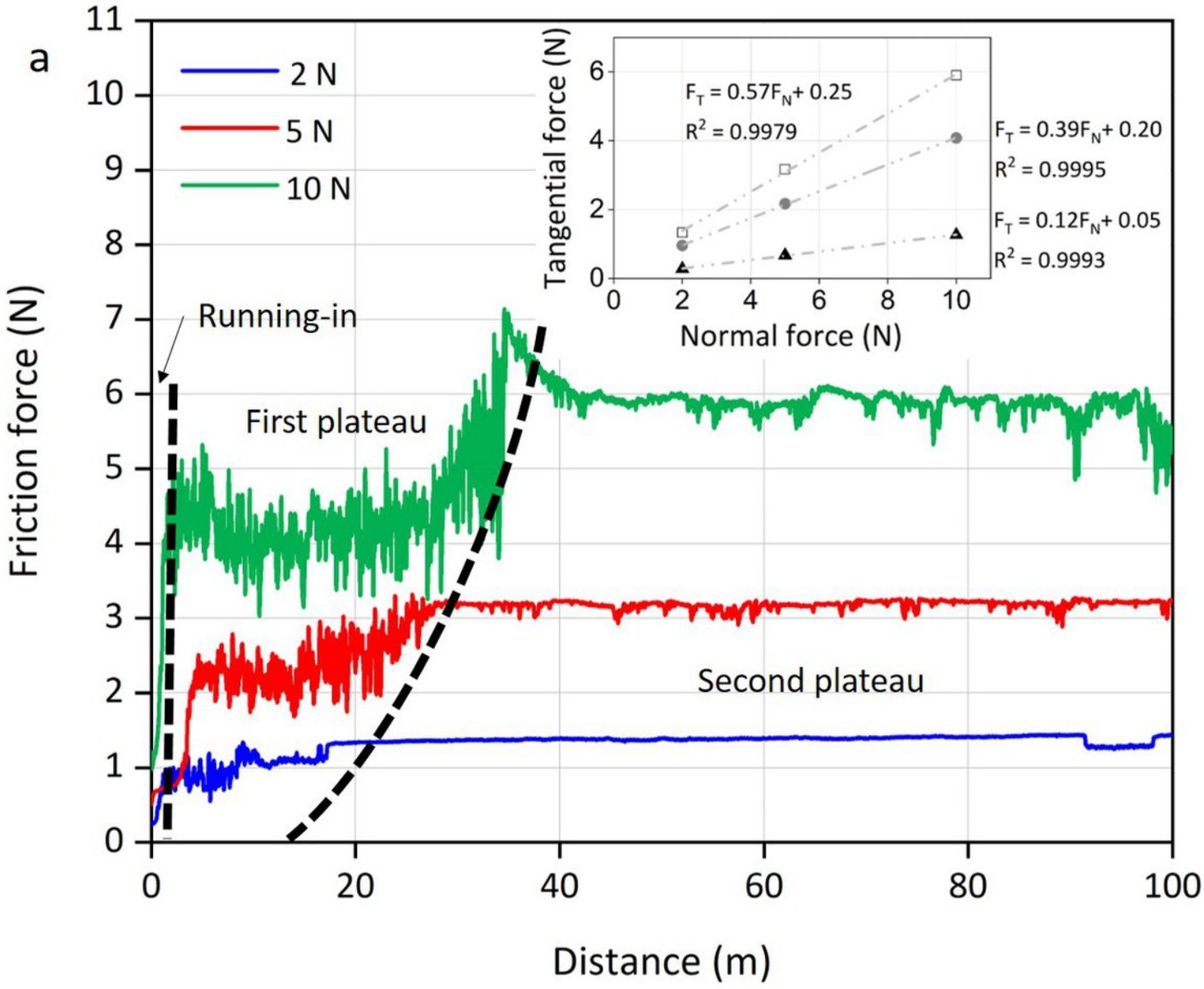
a
2 N
5 N
10 N
Running-in
First plateau
Second plateau
Friction force (N)
Distance (m)
Tangential force (N)
Normal force (N)
$F_T = 0.57F_N + 0.25$
$R^2 = 0.9979$
$F_T = 0.39F_N + 0.20$
$R^2 = 0.9995$
$F_T = 0.12F_N + 0.05$
$R^2 = 0.9993$

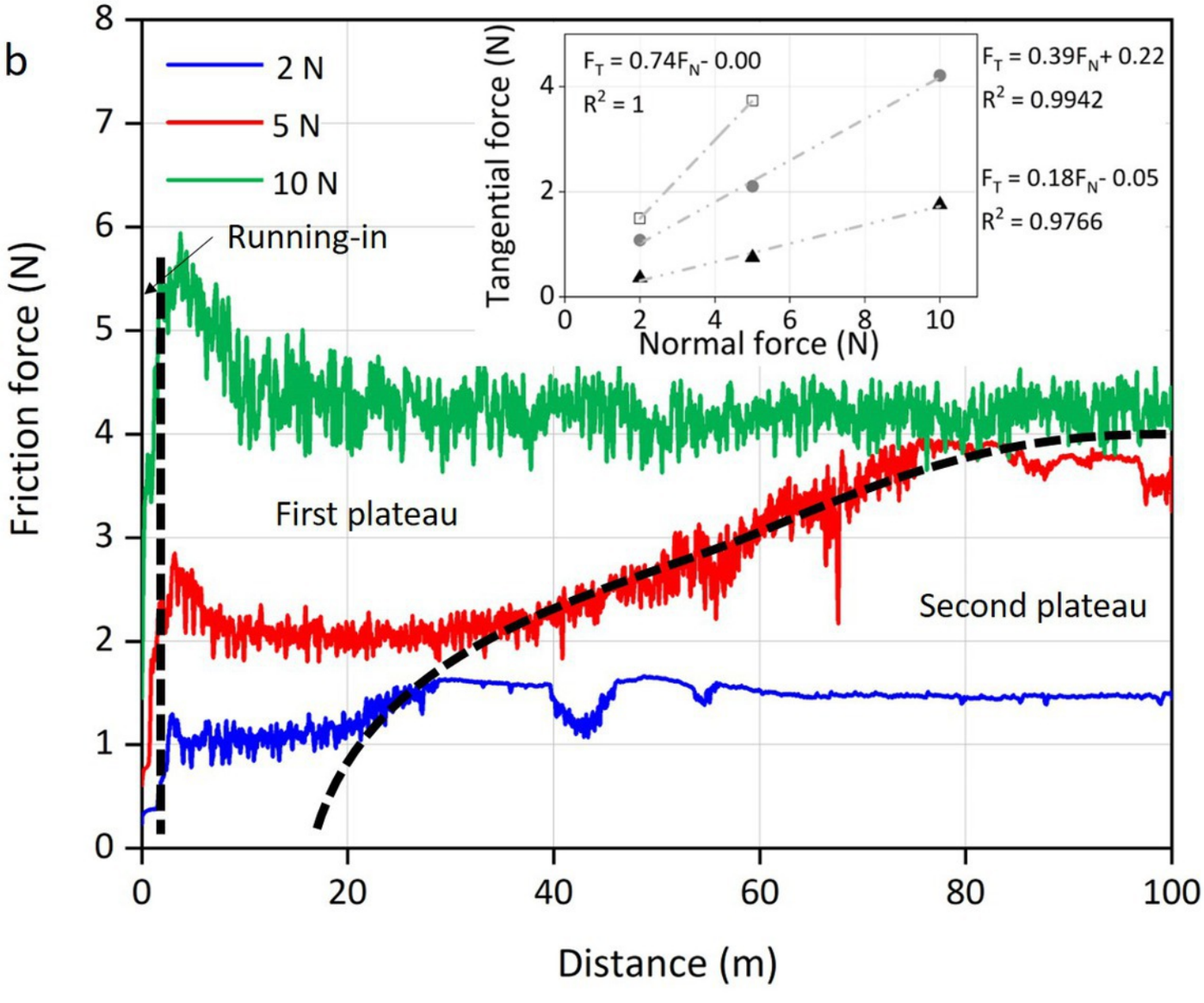
b
2 N
5 N
10 N
Running-in
First plateau
Second plateau
Friction force (N)
Distance (m)
Tangential force (N)
Normal force (N)
$F_T = 0.74F_N - 0.00$
$R^2 = 1$
$F_T = 0.39F_N + 0.22$
$R^2 = 0.9942$
$F_T = 0.18F_N - 0.05$
$R^2 = 0.9766$

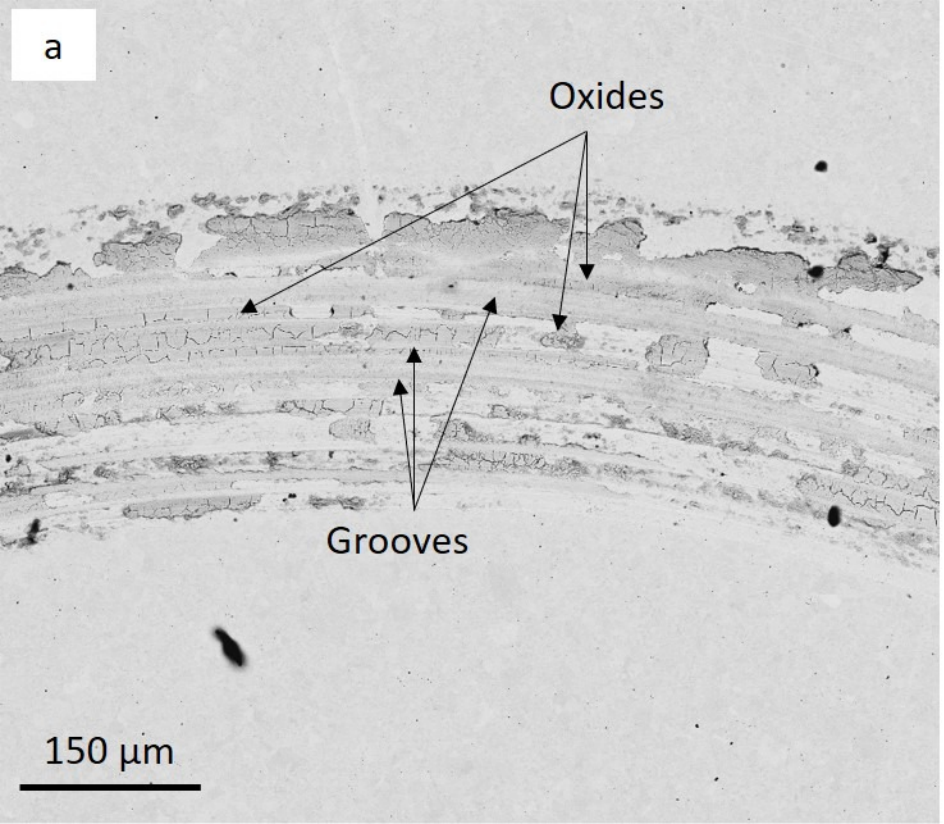
a
Oxides
Grooves
150 µm

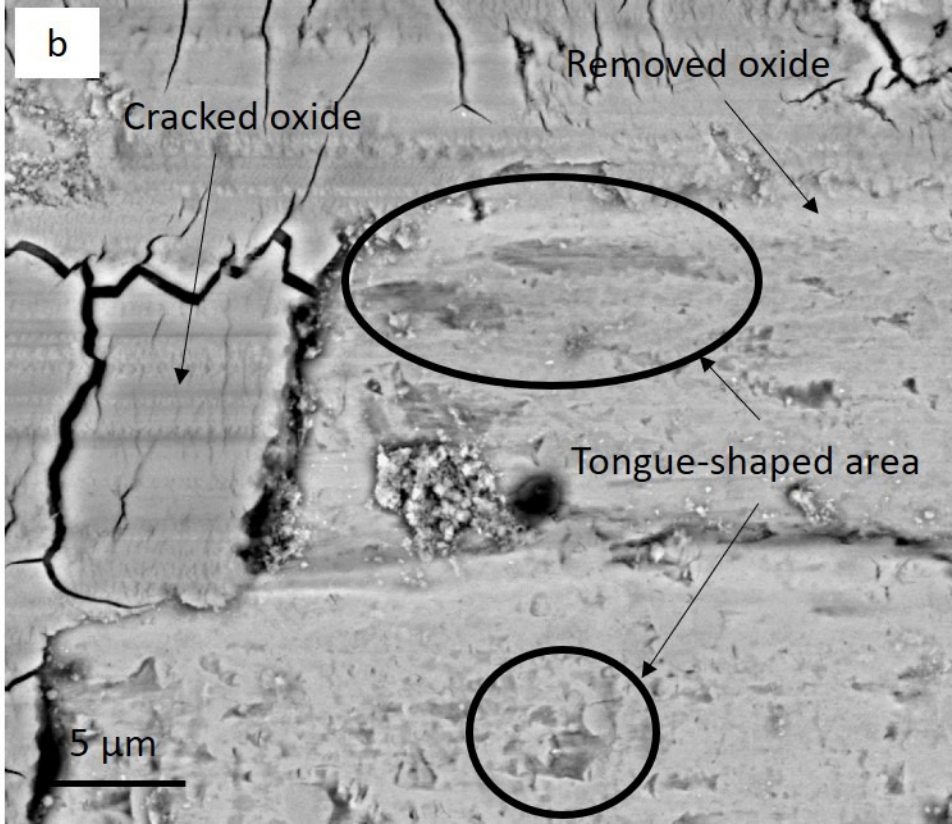
b
Cracked oxide
Removed oxide
Tongue-shaped area
5 µm

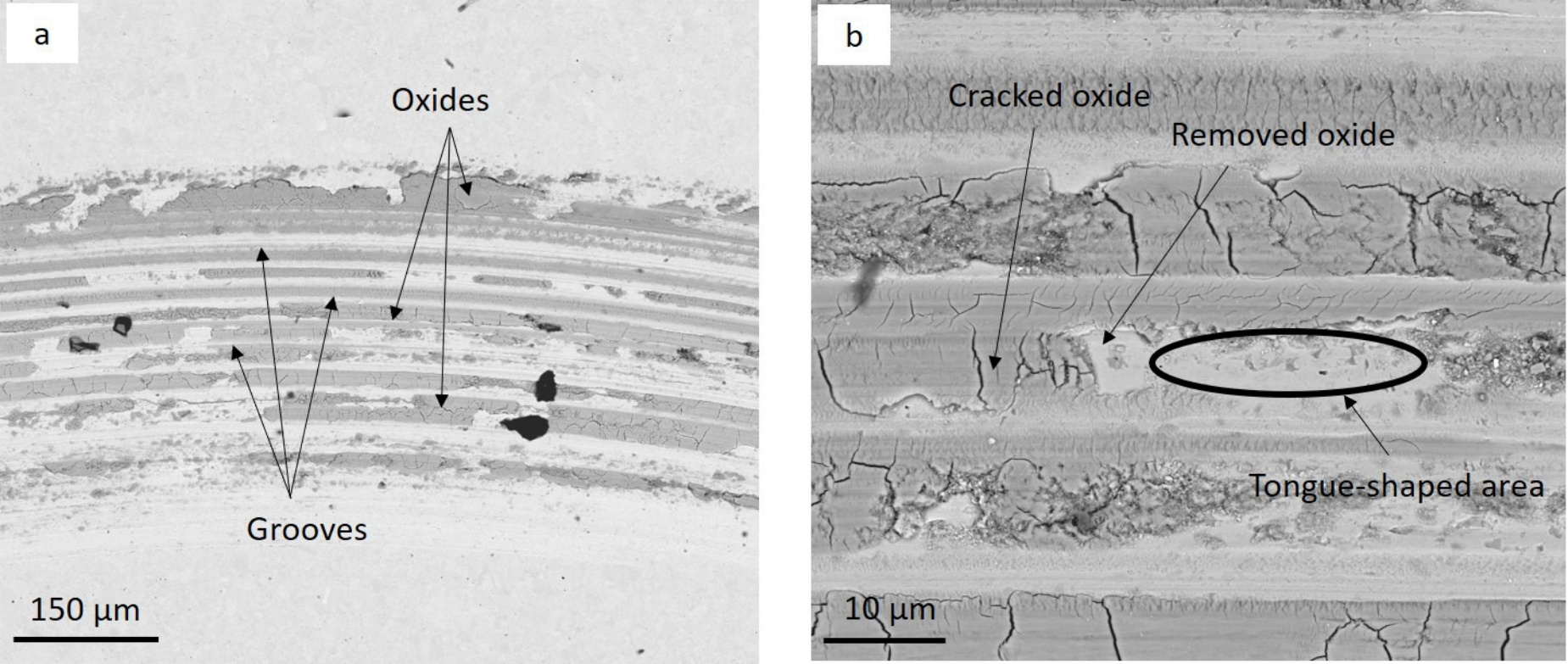
a
Oxides
Grooves
150 µm
b
Cracked oxide
Removed oxide
Tongue-shaped area
10 µm

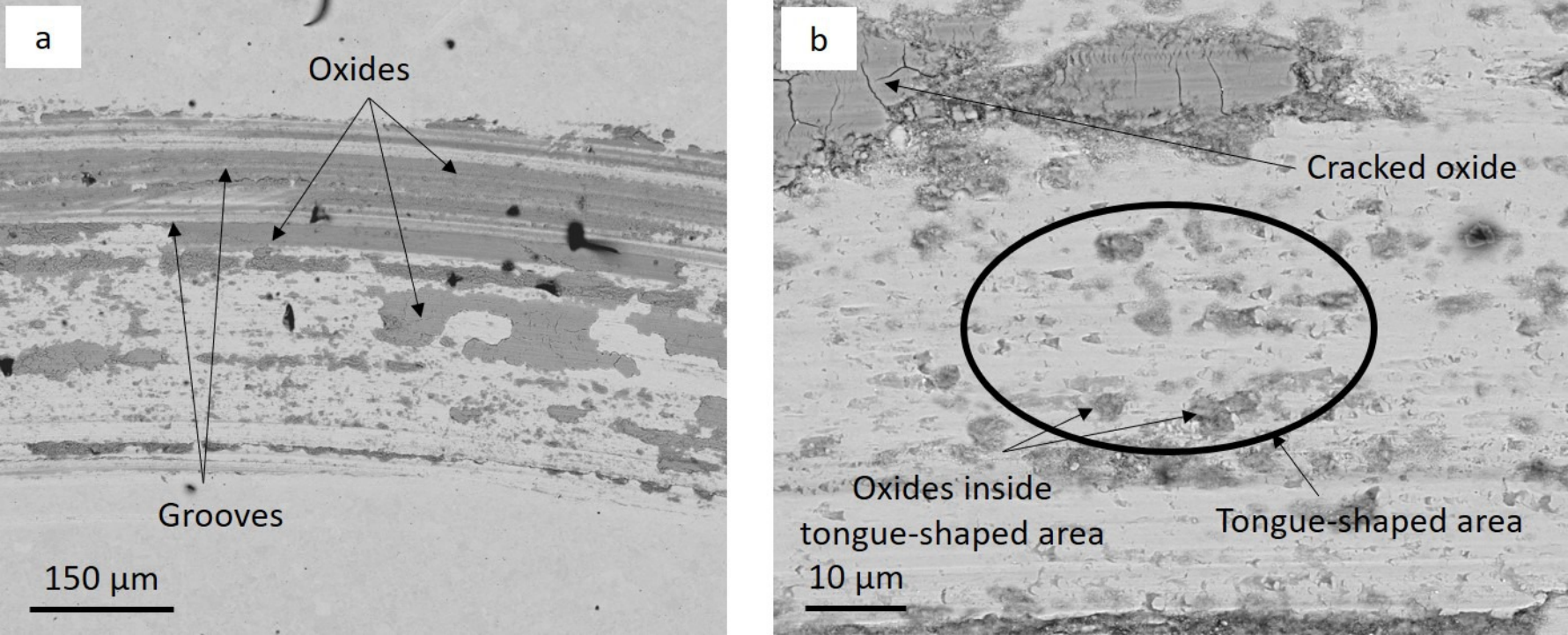
a
Oxides
Grooves
150 µm
b
Cracked oxide
Oxides inside
tongue-shaped area
Tongue-shaped area
10 µm

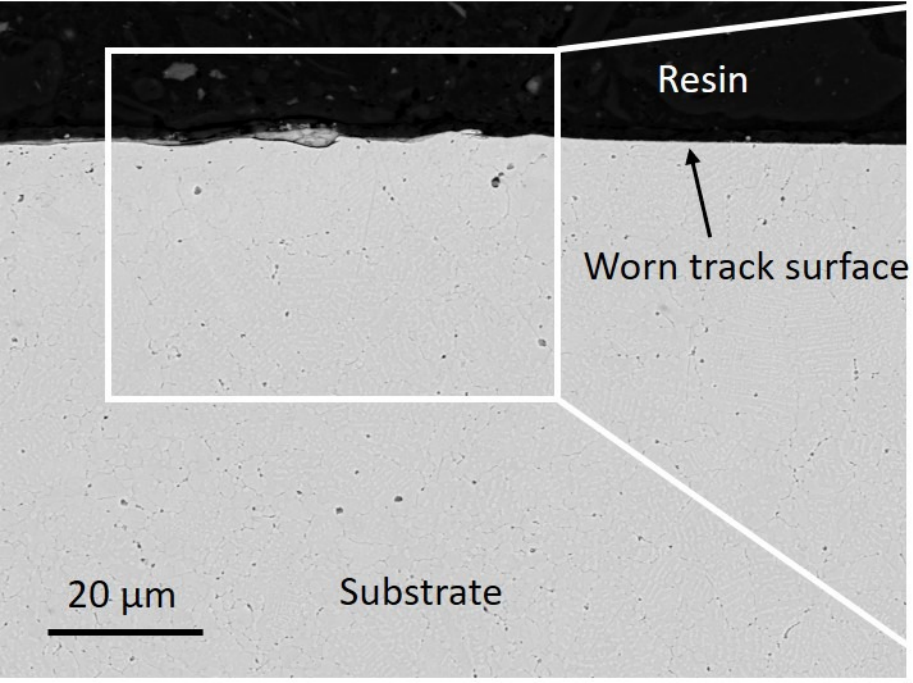
Resin
Worn track surface
20 µm
Substrate

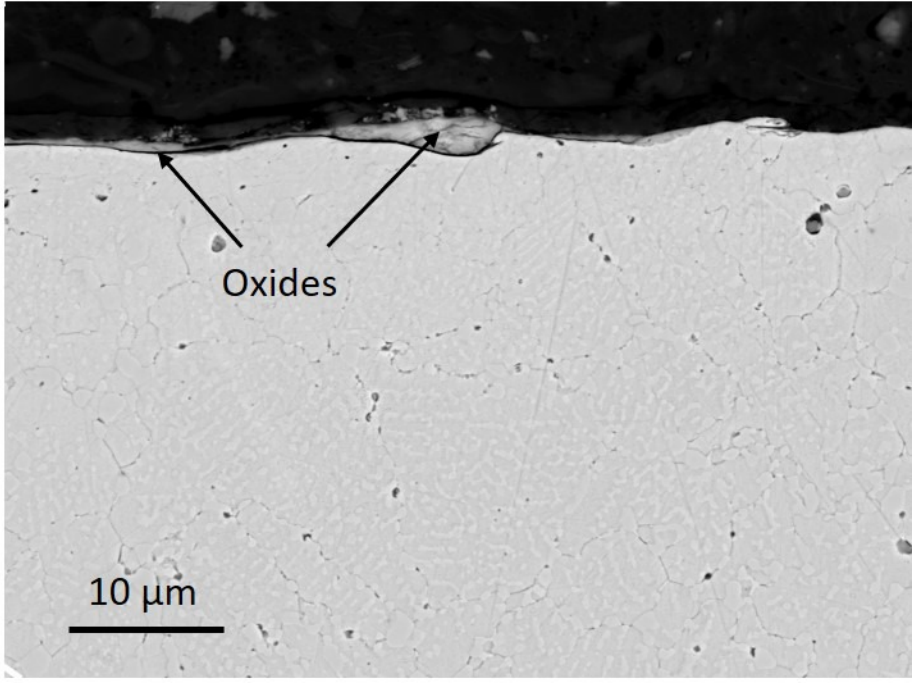
Oxides
10 µm

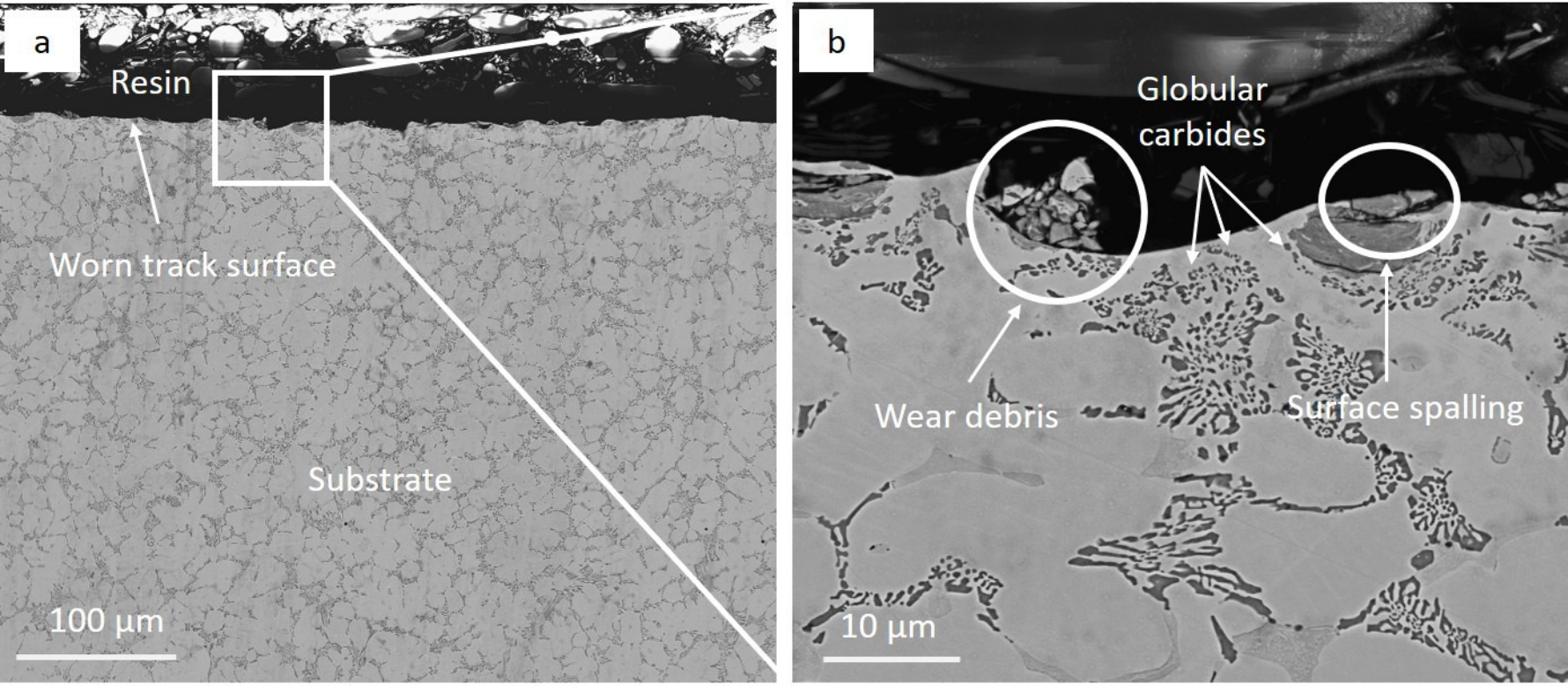
a
Resin
Worn track surface
Substrate
100 µm
b
Globular carbides
Wear debris
Surface spalling
10 µm

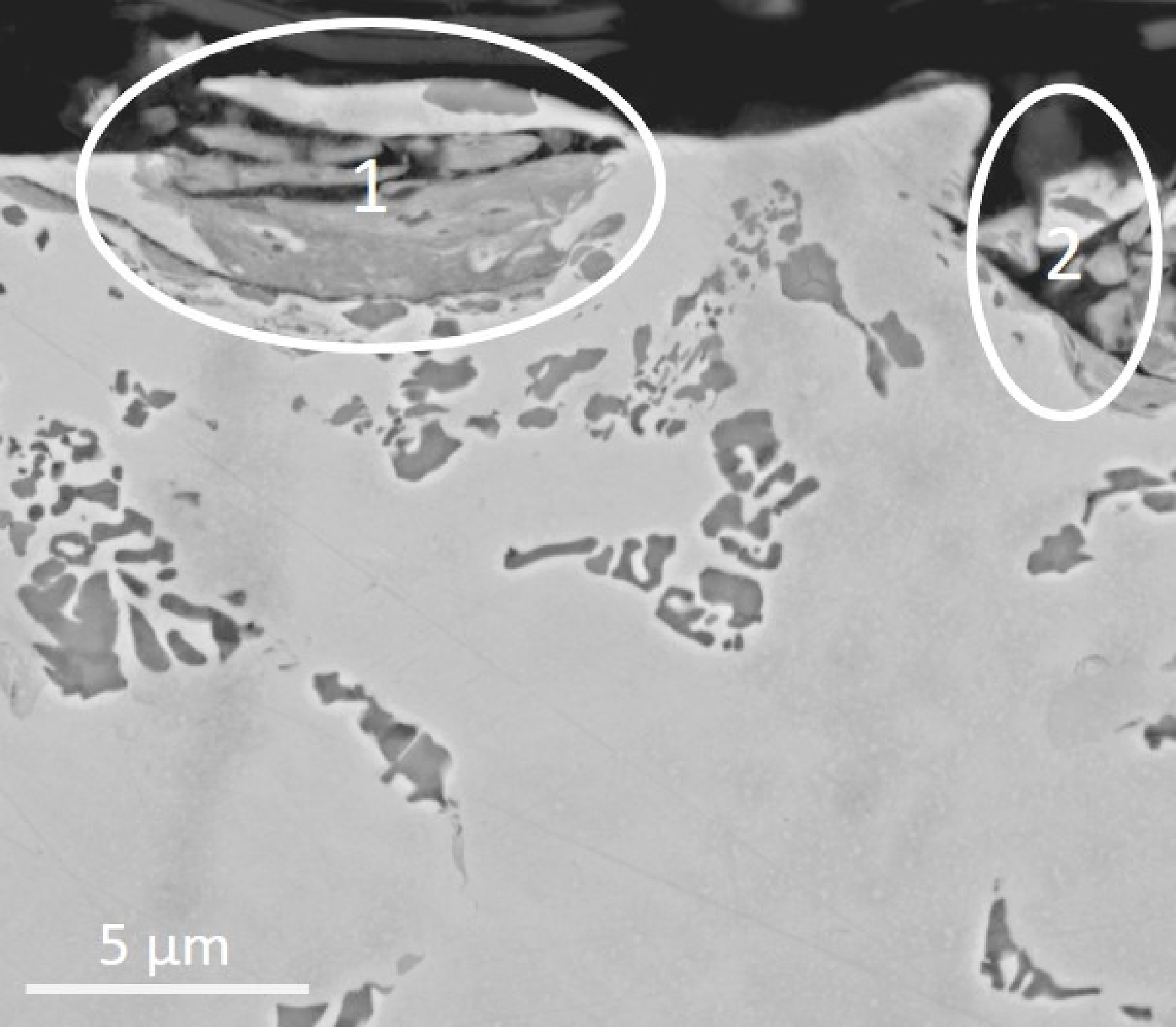
1
2
5 µm